Post-Volcanic Stratospheric Aerosol Decay as Measured by Lidar

M. P. McCORMICK

NASA Langley Research Center, Hampton, VA 23665

T. J. SWISSLER

Systems and Applied Sciences Corporation, Hampton, VA 23666

W. P. CHU AND W. H. FULLER, JR.

NASA Langley Research Center, Hampton, VA 23665

(Manuscript received 28 January 1977, in final form 10 March 1978)

ABSTRACT

Lidar observations of the stratospheric aerosol vertical distribution from October 1974 to July 1976 over midlatitude North America are presented. The results show the sudden increase in the stratospheric aerosol content after the eruption of the Volcán de Fuego and its subsequent decline. The data are presented in terms of lidar scattering ratio profiles, vertically integrated aerosol backscattering, and rawinsonde temperature profiles. In the months immediately following the volcanic eruption, the lidar-derived aerosol structure is correlated with rawinsonde temperature structure showing the stratospheric temperature minimum occurring near the aerosol layer peak. Analysis of the time dependence of the integrated aerosol backscattering and the tropopause altitude indicates an approximate 0.9 correlation between aerosol loading and tropopause pressure. In addition, the integrated aerosol backscattering also showed some correlation with the minimum stratospheric temperature, i.e., a warmer stratospheric minimum is associated with a relatively higher aerosol loading.

The lidar backscatter data also show that rapid decay of the stratospheric aerosol occurred over the late winter to early spring period and that the summer to fall interval was quite stable. For both winter to summer periods of 1975 and 1976 an approximate 40% decrease in the total integrated aerosol backscattering was observed, while from January 1975 to January 1976 a 65% decrease occurred. For the 19-month period from January 1975 to July 1976 the exponential $1/e$ decay time for the integrated aerosol backscattering was 11.6 months.

1. Introduction

Over the past decade, lidar systems have been used extensively in monitoring stratospheric aerosol layers (Fiocco and Grams, 1964; Nishikori *et al.*, 1965; Grams and Fiocco, 1967; Schuster, 1970). One advantage of the lidar technique is that high-resolution vertical measurements of stratospheric aerosol layers can be obtained in real time. These lidar measurements have provided a significant data base for understanding the aerosol loading in the present day stratosphere.

During the 1970's lidar measurements of the stratosphere have shown that aerosol loading reached a low point and quiescent period. Prior to that period, the last major enhancement in loading occurred after the eruption of Agung (8.4°S, 115.5°E) in 1963 (Elterman *et al.*, 1973). In October 1974, however, the Volcán de Fuego in Guatamala (14.5°N, 90.9°W) erupted violently for several days. Large increases in stratospheric aerosols and their related optical effects were observed at different locations in the Northern Hemisphere (McCormick and Fuller, 1975; Fegley and Ellis, 1975; Meinel and Meinel, 1975; Volz, 1975; Russell and Hake, 1977). This infusion of new dust into the stratosphere has been monitored since then with a ruby lidar system located at Hampton, VA (37.1°N, 76.3°W).

This paper will summarize and discuss these lidar observational results for a period of 22 months (October 1974–July 1976), showing the sudden increase in the stratospheric aerosol content after injection and its subsequent decline. Data will be presented in terms of lidar scattering ratio, vertically integrated aerosol backscattering, layer structure and location, and rawinsonde temperature profiles as a function of time.

2. Lidar system and data analysis

The lidar system used in these studies consists of a Q-switched ruby laser ($\lambda = 0.6943\ \mu m$) with mechanical shutter and collimator, which produces an output of 1–2 J with a beam-width divergence of approximately $\frac{1}{2}$ mrad. The mechanical shutter is used to eliminate

laser fluorescence backscatter from nearby the receiver. The receiver utilizes a 48-inch (1.22 m) Cassegrainian-configured $f/10$ telescope mounted on a mobile platform. The backscattered light collected by the telescope is directed through interference filters to a set of photomultiplier tubes. The receiver is interfaced with a minicomputer-based digital data acquisition system for analog-to-digital conversion and storage that can either display near real-time signals averaged over a large number of laser firings or store the digital signals on magnetic tape for detailed analysis with a larger computer.

Using the nearby rawinsonde data from Wallops Island, VA (120 km NE of the lidar system), the molecular backscatter profile for each evening can be computed. The photomultiplier's output voltage as a function of altitude, $V(Z)$, is given by the lidar equation

$$V(Z)=b[f_M(Z)+f_A(Z)]q^2(Z)/Z^2, \tag{1}$$

where $f_M(Z)$ is the molecular backscattering function, $f_A(Z)$ the aerosol backscattering function, $q^2(Z)$ the two-way atmospheric transmittance and b the lidar system calibration factor. Evaluating the ratio

$$Z^2V(Z)/q^2f_M(Z) \tag{2}$$

and substituting from Eq. (1) yield

$$b\frac{f_A(Z)+f_M(Z)}{f_M(Z)}\equiv R'(Z). \tag{3}$$

The lidar total backscatter ratio $R(Z)$, hereafter referred to as the lidar scattering ratio, can then be determined by multiplying $R'(Z)$ with a conversion constant K such that

$$\begin{aligned} R(Z)&=KR'(Z)\\ &=1+f_A(Z)/f_M(Z). \end{aligned} \tag{4}$$

Since the lidar system calibration factor is unknown, the constant K must be determined by normalizing the ratio $R'(Z)$ in an altitude region where backscattering is assumed to be only from molecules. This normalization is performed by choosing the minimum value of

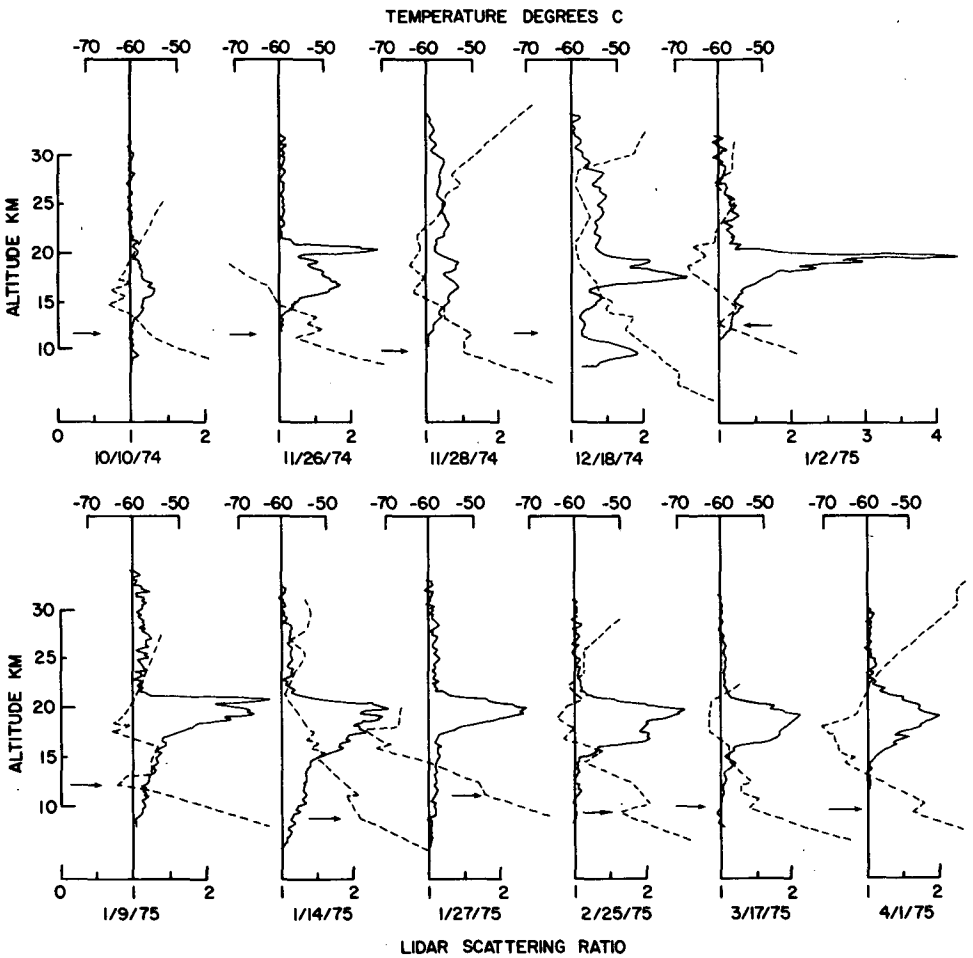

FIG. 1. Vertical profiles of lidar scattering ratios (solid line) and temperature (dashed line) for the period October 1974 to April 1975. The height of the tropopause is indicated by the arrow.

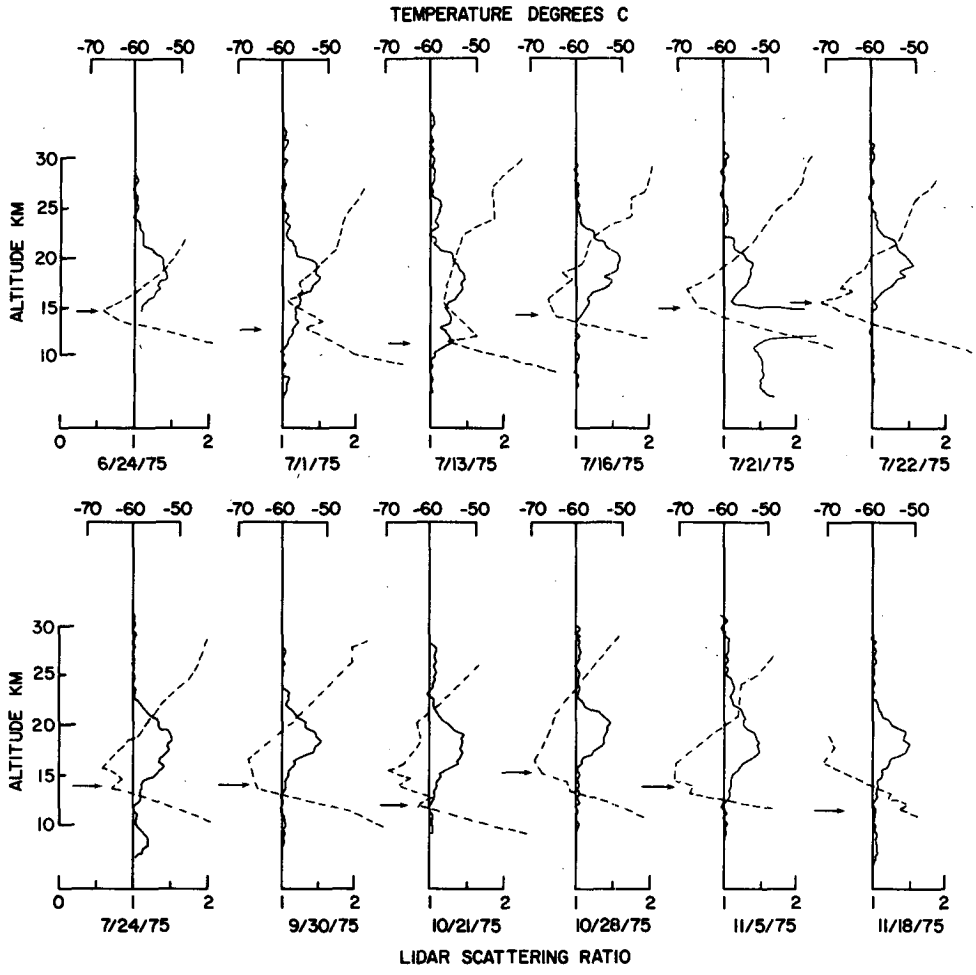

FIG. 2. As in Fig. 1 except for June 1975 to November 1975.

$R'(Z)$ in the altitude range from 24 to 32 km for each averaged profile. In addition, the two-way atmospheric transmittance $q^2(Z)$ has to be assumed. In this paper, the rawinsonde-derived molecular transmission and a moderate volcanic aerosol transmission model at 0.7 μm were used for the lidar data obtained during the initial high aerosol loading period from November 1974 to February 1975. In the subsequent decay period, the aerosol extinction contribution to the transmission was in proportion to the total aerosol loading between 10 and 28 km altitude. The aerosol optical depth used varied between 0.027 for high aerosol loading to 0.008. The sensitivity of the two-way atmospheric transmittance function $q^2(Z)$ to various stratospheric aerosol loadings has been discussed in detail by Russell *et al.* (1976). The maximum error in the ratio $R(Z)$ introduced by the assumed $q^2(Z)$ was estimated to be less than 1%. The lidar scattering ratio and temperature profiles are presented in the next section for the period October 1974–July 1976. Any ratio greater than 1 indicates aerosol scattering.

3. Results and discussion

a. Lidar scattering ratio profiles from October 1974 to July 1976

The vertical profiles of lidar scattering ratio obtained on 35 nights during the 22-month period October 1974–July 1976 are summarized in Figs. 1–3. Typically, 200 laser firings over 2 h are obtained each evening in sets of 30–50 shots. Each profile shown in Figs. 1–3 is the smoothed average of a typical set. It is obtained by vertically smoothing the mean profile of each set with a running average in 0.225 km altitude increments. The lidar scattering ratio profiles are then computed as discussed in the last section. Very little variation in the profile was observed on any one evening. Also shown for comparison in each figure is the corresponding temperature profile obtained from the Wallops' rawinsonde data. The altitude of the tropopause height for each temperature profile is indicated with an arrow. This altitude has been chosen in the customary manner as the height at which a temperature lapse rate of less

than or equal to 2°C km^{-1} for at least 2 km was first obtained.

Fig. 1 begins with the pre-Fuego observation on 10 October 1974. A peak scattering ratio of 1.3 was observed. This peak ratio is considerably higher than values observed during the period 1972–74 which were nominally 1.1 (Russell *et al.*, 1976; Northam *et al.*, 1974). The cause for the unusually high peak ratio on this night is not clear but could be due to the eruption of the Manam Island volcano (4.1°S, 145.3°E) which underwent a period of eruptive activity between May and later September 1974 (Gras, 1976). In any event, it is small compared to the ratios that followed the Fuego eruption. The 26 November 1974 profile in Fig. 1 is the first published lidar observation of the Fuego injection (McCormick and Fuller, 1975). A narrow peak layer at 20 km accompanied by a secondary broad layer centered at 16 km was observed. Two days later on 28 November the dust seemed to have spread in altitude from 12 km to over 30 km. The integrated amount of dust which will be discussed in a later section is, however, quite significant compared to pre-Fuego levels. The observation on 18 December also shows a very large enhancement in stratospheric dust and a multilayered structure. The vertical distribution of dust during the first two weeks of January 1975 were generally multi-layered with sharp, narrow peaks. A peak scattering ratio of 4.2 was observed on 2 January, the largest ever recorded by the authors. The vertical profiles show the same large variations as in the November and December profiles but with less variation above the main peak (above 20 km), with the peak ratio slowly decreasing during the month. The observations from February to April 1975 show that the multilayered profiles have merged into a more or less vertically homogeneous broad layer centered at 19 km. The peak scattering ratio during this period was approximately 2. Fig. 2 shows the main layer to be stable with a peak scattering ratio of 1.5 throughout the summer and fall of 1975. Fig. 2 also includes data taken in the month of July 1975, at Kansas City, MO (39°N, 95°W). The vertical profiles were similar to those obtained at Hampton, VA, during this summer period. Fig. 3 shows the vertical profiles from December

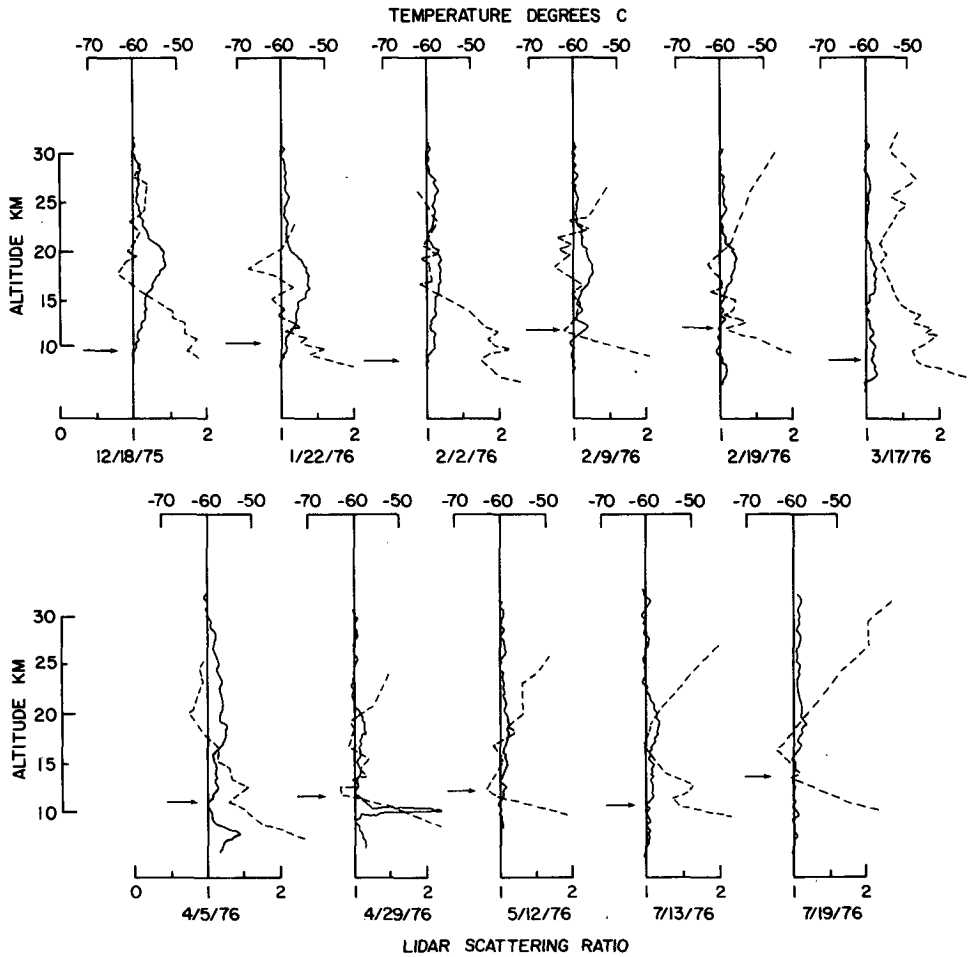

FIG. 3. As in Fig. 1 except for December 1975 to July 1976.

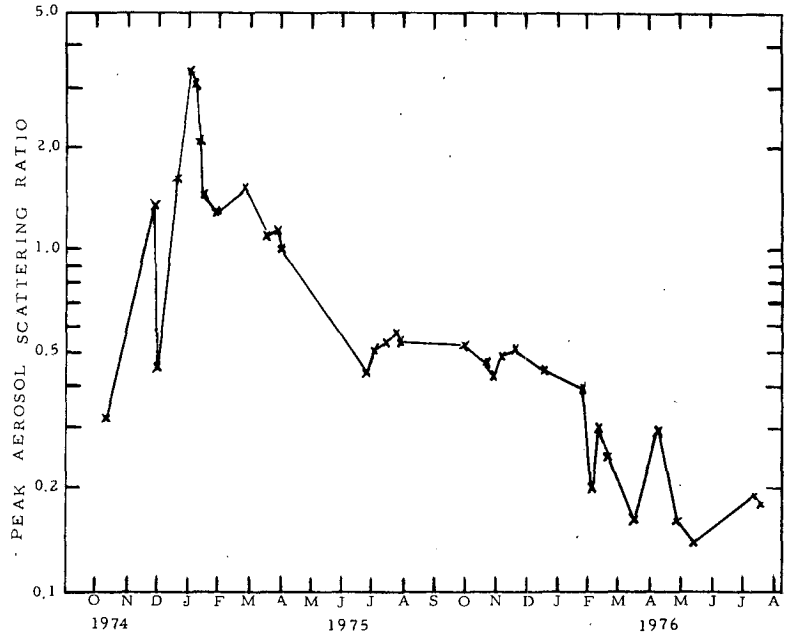

FIG. 4. Time variation of the peak aerosol scattering ratio, $\max(R-1)$, from October 1974 to July 1976.

1975 to July 1976. The stratospheric dust loading gradually declined as the peak ratio dropped from a value of 1.5 to 1.2. In March 1976, the vertical profile returned to the pre-Fuego value of 10 October 1974.

b. Temperature versus aerosol structure

In the eight months following the eruption when the aerosol loading was high, the temperature structure is correlated with the lidar-derived dust layers and its finestructure. In general, the minimum temperature is always included in the peak dust layer, and, in a number of cases, the finestructure of the dust layer is well correlated with the fine temperature structure (cf. 28 November 1974, 2 January 1975, 1 April 1975, etc.). These findings are in general agreement with the heterogeneous-heteromolecular particle formation model of Hamill *et al.* (1977) that describes the region of the stratosphere where aerosol formation is expected to occur. According to the model, sulfuric acid aerosols are formed by the condensation of H_2SO_4 and H_2O gases onto preexisting particles near stratospheric temperature minima.

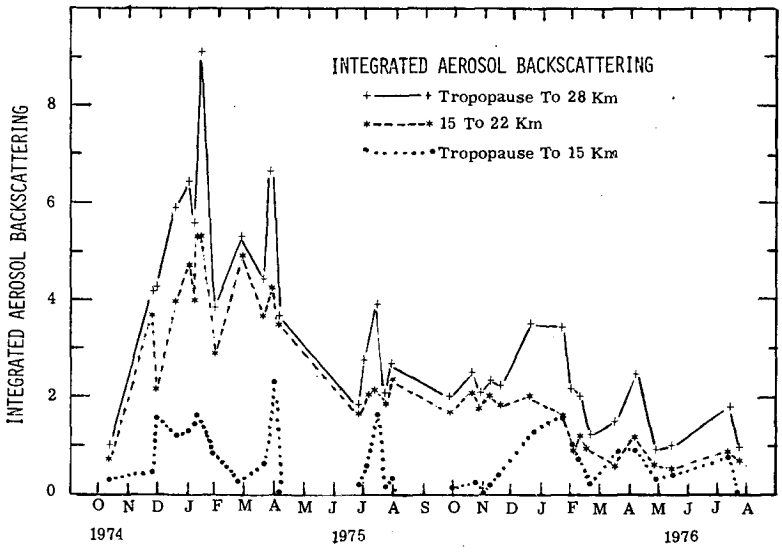

FIG. 5. Time variation of the integrated aerosol backscattering for given stratospheric layers from October 1974 to July 1976.

c. Time history

The time variation of the stratospheric dust layer observed from these lidar profiles can be illustrated by plotting the peak aerosol backscattering ratio as a function of time as shown in Fig. 4, and the integrated stratospheric aerosol backscattering as a function of time as shown in Fig. 5. The peak aerosol backscattering ratio is defined as

$$\max[R(Z)-1], \tag{5}$$

where $R(Z)$ is the lidar scattering ratio defined by Eq. (4). The integrated aerosol backscattering is defined as

$$\int_{h_T}^{28} [R(Z)-1] f_M(Z) dZ, \tag{6}$$

where h_T is the height (km) of the tropopause and $f_M(Z)$ the molecular backscattering function based on near real-time rawinsonde data. This integral has been normalized to the value obtained from the lidar data of 10 October 1974.

The time variation in the integrated aerosol backscattering can be examined in more detail by dividing the lower stratosphere into three regions: 1) a region from the tropopause up to 15 km where periodic variations have been observed by others in the winter-spring aerosol profiles (Hofmann *et al.*, 1975); 2) the region between 15 and 22 km where the main stratospheric dust layer is observed; and 3) the altitude range from the tropopause to 28 km. These curves are shown in Fig. 5. The aerosol content of the 15–22 km layer appears to be dominant in the total integrated backscattering up to 1976. The behavior of this layer and the peak ratio shown in Fig. 4 demonstrate the buildup of the aerosols immediately after the volcanic eruption, the initial weekly fluctuations that were observed, and the subsequent decay to values representative of pre-Fuego eruption conditions. Note that there were large decreases during both winter to spring periods and relatively little change in the summer of 1975. After the initial injection period, the sharp variations or secondary peaks that appear in the total integrated amount are coincident with the behavior of the aerosol content from the tropopause to 15 km. By January 1976, the 15–22 km layer was no longer the dominant contributor to the total integrated amount. It should be pointed out that erroneous aerosol profiles could be deduced from lidar backscatter if one normalized the lidar data at a fixed altitude slightly above the local tropopause in periods of high volcanic activity.

The analysis of the time variation of the stratospheric aerosol content seems to describe not only the decay of the aerosol layer but also certain periodic variations in the description of the aerosol layer that are at least partially seasonal. If specific meteorological parameters are plotted and compared with the integrated aerosol backscattering, correlations are obtained with the seasonal fluctuations in the aerosol layer. This is shown in Fig. 6 where the integrated aerosol backscattering for the tropopause to 28 km is replotted with tropopause height and the minimum stratospheric

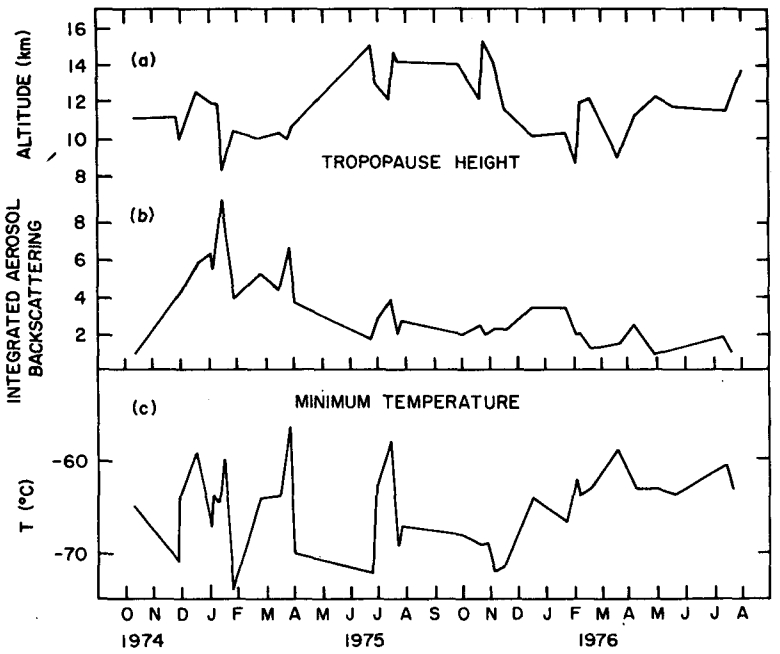

FIG. 6. Time variation of (a) tropopause height, (b) integrated aerosol backscattering for the tropopause to 28 km from October 1974 to July 1976 and (c) stratospheric minimum temperature.

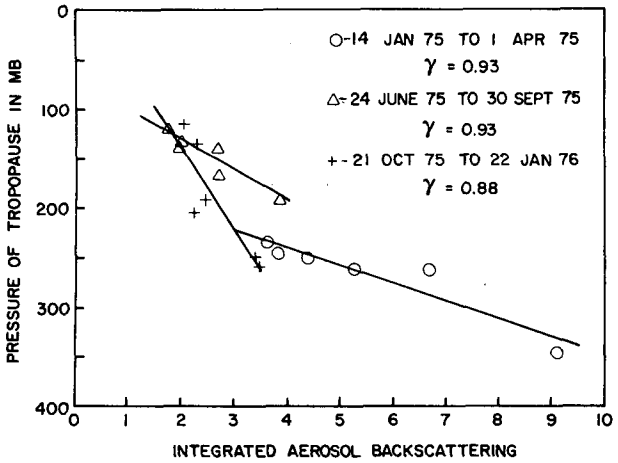

FIG. 7. Correlation coefficients for integrated aerosol backscattering versus observed tropopause pressure for the three indicated time periods. Straight lines are least-squares fit to the data.

temperature. There exists a high degree of correlation between the integrated aerosol backscattering and the tropopause height such that as the height of the tropopause decreases, the total integrated backscattering increases and vice versa. This correlation is demonstrated in Fig. 7 where the integrated aerosol backscattering from the tropopause to 28 km is plotted versus the tropopause pressure. The effect due to the decay of the aerosol loading is minimized by separating the data into three seasonal periods; January–April 1975, summer of 1975 and October 1975–January 1976. The three straight lines in Fig. 7 are least-square fits to the data. The correlation coefficients are 0.93 for the first two time periods with a significance level of 1% and 0.88 for the third time period with a 5% significance level. This high degree of correlation for the integrated aerosol backscattering and the tropopause pressure agrees well with the findings of Hofmann *et al.* (1975). Analysis of the data from February 1976 to July 1976, however, shows poor correlation. This is to be expected since during this time period the peak lidar scattering ratios are consistently below the value of 1.3. Large errors in the determination of f_A for profiles with these low ratios would produce large uncertainties in estimating the integrated aerosol backscattering (Russell *et al.*, 1976). In addition to the correlation with the total region (tropopause to 28 km),

TABLE 1. Correlation coefficients γ for integrated aerosol backscattering versus tropopause pressure.

Dates	Layer		
	Tropopause–15 km	15–22 km	Tropopause–28 km
14 Jan–1 Apr 75	0.88	0.77	0.93
24 Jun–9 Sept 75	0.95	0.47	0.93
24 Oct 75–22 Jan 76	0.94	0.06	0.88

TABLE 2. Correlation coefficient γ for integrated aerosol backscattering versus minimum stratospheric temperature.

Dates	Layer		
	Tropopause–15 km	15–22 km	Tropopause–28 km
14 Jan–1 Apr 75	0.60	0.75	0.74
24 Jun–9 Sept 75	0.95	0.52	0.95
24 Oct 75–22 Jan 76	0.77	0.68	0.86

a similar high degree of correlation of ~0.9 is obtained for the region from the tropopause to 15 km but no significant correlation is obtained for the 15–22 km region that contains the peak aerosol layer (see Table 1). This correlation of variation in the integrated (tropopause to 28 km) aerosol backscattering coincident with tropopause height could be due to a seasonal adjustment of the mean tropopause height, to transport mechanisms such as the large-scale turbulent mixing process described by Reiter (1975), or to other unknown mechanisms.

An additional correlation in the data is recognized in the year after the first indication of the eruption between the warmest minimum stratospheric temperature and the peaks in the integrated aerosol backscattering. The minimum stratospheric temperature appears at its relative warmest for those times where the integrated backscattering is at a local maximum. This correlation is demonstrated in Fig. 8 where the integrated aerosol backscattering is plotted versus the minimum stratospheric temperature for the same three time periods of Fig. 7. The correlation coefficient is calculated from a linear least-square fit to the data. For the three periods, they were 0.74, 0.95 and 0.86 at significance levels of 10, 1 and 5%, respectively, indicating correlation between warmer minimum temperatures and increased integrated aerosol backscattering. These correlations are given in Table 2 for each altitude layer as previously defined. It should be pointed out, however, that warmer stratospheric temperatures are not necessarily due to

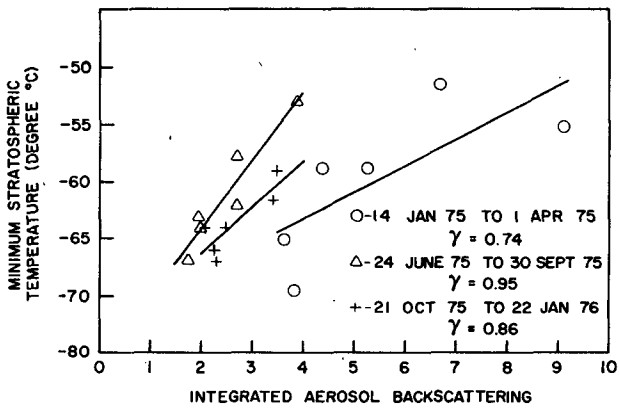

FIG. 8. As in Fig. 7 except for observed stratospheric minimum temperature.

TABLE 3. Exponential (1/e) decay times in months.

	Jan 75–Jun 75	Jul 75–Dec 75	Jan 76–Jul 76	Jan 75–Jul 76
Peak	3.4	37.0	12.9	7.5
Integrated aerosol backscattering				
15–22 km	6.8	67.0	11.8	9.3
Tropopause–28 km	4.9	95.0	14.0	11.6

heating effects of volcanic aerosols but could be due to the advection of warm aerosol-laden air. These observations point out the importance of a complete description of the meteorological variables when drawing conclusions from such measurements.

d. Decay times

Decay rates have been calculated for the peak aerosol backscattering and integrated aerosol backscattering by fitting an exponential curve to the data of Figs. 4 and 5. These decay rates are summarized in Table 3. The decay rates are variable depending on the season and the elapsed time from the eruption as can be seen by comparing the different columns. Generally, rapid decay of stratospheric aerosol occurs over the late winter to early spring period, while the summer to fall period is quite stable. These data point out the sensitivity in decay time with observational period and the obvious importance in taking this into consideration when determining trends or consequences.

For both winter to summer periods of 1975 and 1976, the lidar data showed an approximately 40% decrease in the integrated aerosol backscattering. This is the expected time of maximum midlatitude mixing. The decrease over the period January 1975–January 1976 is approximately 65%. This agrees roughly with Reiter's (1975) estimate of 73% annual outflow of stratospheric air mass over the Northern Hemisphere consisting of stratospheric-tropospheric exchange of 38% due to Hadley cell circulation, 20% due to the jet stream activity, and 15% due to seasonal changes in the tropopause heights and transport into the Southern Hemisphere.

4. Concluding remarks

This paper presents fixed-location lidar data over 22 months after a volcanic eruption. Understanding the inherent limitations and interpretations of such measurements it is obvious that lidar is a useful tool in delineating stratospheric aerosol content. It is also evident that care should be taken in the use of data taken over short periods of time since large variations have been shown to exist seasonally. In addition, lidar normalization techniques must take into consideration variations in vertical aerosol profiles. Finally, this fixed-location data set points to the enhanced usefulness of aerosol measurements taken over larger geographic areas from aircraft or satellite platforms. Such widespread measurements would make significant contributions to the understanding of the stratosphere.

REFERENCES

Elterman, L., R. B. Toolin and J. D. Essex, 1973: Stratospheric aerosol measurements with implications for global climate. *Appl. Opt.*, **12**, 330–337.

Fegley, R. W., and H. T. Ellis, 1975: Lidar observations of a stratospheric dust cloud layer in the tropics. *Geophys. Res. Lett.*, **2**, 139–141.

Fiocco, G., and G. Grams, 1964: Observation of aerosol layer of 20 km by optical radar. *J. Atmos. Sci.*, **21**, 323–324.

Grams, G., and G. Fiocco, 1967: The stratospheric aerosol layer during 1964 and 1965. *J. Geophys. Res.*, **72**, 3523–3542.

Gras, J. L., 1976: Southern Hemisphere mid-latitude stratospheric aerosol after the 1974 Fuego eruption. *Geophys. Res. Lett.*, **3**, 533–536.

Hamill, P., O. B. Toon and C. S. Kiang, 1977: Microphysical processes affecting stratospheric aerosol particles. *J. Atmos. Sci.*, **34**, 1104–1119.

Hofmann, D. J., J. M. Rosen, T. J. Pepin and R. G. Pinnick, 1975: Stratospheric aerosol measurements I: Time variations at northern latitudes. *J. Atmos. Sci.*, **32**, 1446–1456.

McCormick, M. P., and W. H. Fuller, Jr., 1975: Lidar measurements of two intense stratospheric dust layers. *Appl. Opt.*, **14**, 4–5.

Meinel, A. S., and M. P. Meinel, 1975: Stratospheric dust aerosol event of November 1974. *Science*, **188**, 477–478.

Nishikori, K., T. Kshida, K. Uchikura, K. Muranaga, M. Ichinose, Y. Masuda, T. Nagatake, M. Hirono and T. Igaraski, 1965: On observations of the upper atmosphere by ruby laser. *J. Radio Res. Lab.*, **12**, 213–222.

Northam, G. B., J. M. Rosen, S. H. Melfi, T. J. Pepin, M. P. McCormick, D. J. Hofmann and W. H. Fuller, Jr., 1974: A comparison of dustsonde and lidar measurements of stratospheric aerosols. *Appl. Opt.*, **13**, 2416–2421.

Rieter, E. R., 1975: Stratospheric-tropospheric exchange processes. *Rev. Geophys. Space Phys.*, **13**, 459–474.

Russell, P. B., and R. D. Hake, Jr., 1977: The post-Fuego stratospheric aerosol: Lidar measurements, with radiative and thermal implications. *J. Atmos. Sci.*, **34**, 163–177.

——, W. Viezee, R. D. Hake, Jr., and R. T. H. Collis, 1976: Lidar observations of the stratospheric aerosol: California, October 1972 to March 1974. *Quart. J. Roy. Meteor. Soc.*, **102**, 675–695.

Schuster, B. G., 1970: Detection of aerosol layers by optical radar (lidar). *J. Geophys. Res.*, **75**, 3123–3132.

Volz, F. E., 1975: Volcanic twilights from the Fuego eruption. *Science*, **189**, 48–50.